Zhang *et al. Dis Prev Res* 2024;3:9
DOI: 10.20517/dpr.2024.08

Disaster Prevention and Resilience

Research Article

Open Access

Wind turbine foundation ring fatigue reliability analysis under wind-load using SCADA system

Zhenhao Zhang, Yu Liu, Wenbiao Li

School of Civil Engineering, Changsha University of Science and Technology, Changsha 410114, Hunan, China.

Correspondence to: Prof. Zhenhao Zhang, School of Civil Engineering, Changsha University of Science and Technology, 960 Wanjiali South Road, Changsha 410114, Hunan, China. E-mail: zhangzhenhao@csust.edu.cn

How to cite this article: Zhang Z, Liu Y, Li W. Wind turbine foundation ring fatigue reliability analysis under wind-load using SCADA system. *Dis Prev Res* 2024;3:9. https://dx.doi.org/10.20517/dpr.2024.08

Received: 8 Jun 2024 **First Decision:** 27 Aug 2024 **Revised:** 8 Sep 2024 **Accepted:** 25 Sep 2024 **Published:** 30 Sep 2024

Academic Editor: Qingshan Yang **Copy Editor:** Fangling Lan **Production Editor:** Fangling Lan

Abstract

Under the action of wind load, the foundation ring of the fan will generate stress concentration and alternating stress, leading to fatigue failure. Based on the average wind speed obtained from the supervisory control and data acquisition (SCADA) system, the orthogonal expansion method of random pulsating wind field and the number theory point selection method are used to calculate and simulate the corresponding pulsating wind speed time series, and then calculate the wind speed time series and wind load time series. Based on the ABAQUS finite element software, a model of a 5 MW wind turbine is established. The modal analysis is used to obtain the modal vibration pattern and the intrinsic frequency to verify the reasonableness of the structural modeling. Subsequently, the wind load time series is applied to the wind turbine model to obtain the stress time series using instantaneous modal dynamic analysis (Modal dynamics). The stress time series at the location of maximum stress concentration in the foundation ring is extracted, and the stress time series with the same stress amplitude is obtained through conversion, which has Wiener characteristics. After obtaining the stress amplitude using the rainflow counting method, the fatigue reliability is calculated based on the structural fatigue reliability analysis method considering the threshold crossing duration of the random process. This research holds reference significance for the calculation of fatigue reliability under approximate working conditions.

Keywords: Wind turbine structure, service safety, fatigue reliability, orthogonal expansion, stress stochastic process

INTRODUCTION

Most collapse accidents of wind turbine structures are caused by fatigue damage to the concrete foundation

or connecting bolts of the wind turbine under wind load, leading to noticeable sliding displacement and structural collapse. Currently, although a large amount of analysis has been conducted on the reliability of wind turbine structures, the various uncertainties present in the natural environment and the operation process make it difficult to accurately assess the fatigue reliability of wind turbine structures using constant reliability statistical indicators. Therefore, research on the fatigue reliability of wind turbines is relatively limited. Therefore, it is of great practical significance and economic value to use real-time monitoring data from supervisory control and data acquisition (SCADA) systems to establish a structural model of wind turbines and conduct fatigue reliability analysis. Condition monitoring is an important means to improve the operational safety of wind turbines and is of great significance for the safe and efficient utilization of the turbine structure[1-9]. Monitoring techniques for wind turbine structures mainly include ultrasonic testing, thermal imaging, process parameter monitoring, performance parameter monitoring, and X-ray imaging techniques. Currently, the most widely used real-time monitoring system for wind turbine structures is the SCADA system, which can monitor the operation status of all components or subsystems of the turbine structure in real-time. It integrates information collection, condition monitoring, and parameter adjustment, providing technical support for the long-term safe operation of wind turbine structures.

The SCADA system of wind turbines has the capability of real-time monitoring and data acquisition, and many scholars have utilized this system to solve problems that are more in line with actual operating conditions. Kusiak *et al.* used historical operating data of wind turbine structures to select relief algorithm characteristic parameters for the "three-blade asymmetry" and "abnormal pitch angle" faults of the variable pitch system[10]. Gill *et al.* used SCADA system operating data to establish a probability model of the power curve of the wind turbine structure based on Copula functions, effectively monitoring early signs of blade degradation, yawing, and variable pitch system faults[11]. Kusiak *et al.* used the Hotelling's T2 statistical method to analyze the active power operating data of the turbine, identifying the operating state of the entire unit[12]. Zaher *et al.* developed an automatic anomaly detection system that identifies early turbine faults through automatic analysis of online SCADA data[13]. Garcia *et al.* used SCADA operating data to establish a gearbox temperature model, evaluating the health condition of the gearbox by continuously monitoring the prediction confidence interval of the model[14]. Yang *et al.* proposed the use of SCADA data monitoring technology to assess the health status of different operating conditions, detect early faults in blades and drive systems, and track their further deterioration[15]. Zhang *et al.* proposed a dynamic model sensor approach for wind turbine fault detection based on SCADA data, as the changes in measurement capabilities of the hardware sensors used in current SCADA systems often fail to provide reliable early warnings[16]. Zhang *et al.* proposed health condition evaluation indicators for wind turbine units based on the relationship with SCADA (monitoring and data acquisition) data[17]. Tang *et al.* developed a novel fault diagnosis and prediction method based on support vector regression models using data obtained from the monitoring and data acquisition system (SCADA) of wind turbines[18]. Liu developed a new state monitoring and fault isolation system to address inherent issues in SCADA data analysis, including low sampling rates, time-varying operating conditions of wind turbine units, and a lack of historical fault data[19].

In recent years, there have been frequent incidents of wind turbine foundation ring detachment from the surrounding concrete or damage to the connection between the foundation and the upper tower structure. These incidents have resulted in excessive tower oscillation, turbine alarms, shutdowns, and even collapses, causing significant economic losses that are difficult to estimate. The main cause of these problems is excessive fatigue loads. Therefore, the fatigue reliability analysis of wind turbine structures has attracted widespread attention from researchers. For example, Velarde *et al.* proposed a reliability-based framework for calibrating the partial safety factors of fatigue in offshore wind turbine concrete structures[20]. They used a fully integrated aeroelastic model to estimate the load on offshore wind turbines considering the statistical

distribution of turbulence intensity. Based on existing fatigue tests, they established a fatigue reliability model for concrete and applied it to two numerical examples. The results showed that the recommended partial safety factors for materials in the Det Norske Veritas (DNV) standard can be reduced for offshore concrete structures without compromising structural safety. Wang *et al.* studied the fatigue damage of offshore wind turbine foundations using stress accumulation methods and found that the coupling effect of wind and wave loads has a significant impact on the overall fatigue damage of wind turbine structures[21]. Fu *et al.* investigated the fatigue reliability of tower flanges and bolts[22]. Zhu *et al.* proposed a new probabilistic modeling framework for analyzing the long-term fatigue reliability of wind turbine units[23]. Due to the high computational cost of dynamic response simulations in different environmental scenarios, this framework aims to reduce computational costs and improve the feasibility of long-term fatigue evaluation. Li *et al.* used a multidimensional finite element method to calculate the fatigue load history of large wind turbine gear systems under the coupling mechanism of elastic behavior[24]. By conducting low-cycle fatigue tests on the gears and using the lifetime distribution transformation method, they obtained the probability fatigue strength of the gear teeth. They thoroughly explored the inherent characteristics of wind turbine gear systems in functional implementation and established a fatigue reliability assessment model for the system. They also constructed a mapping path between the global structural unit of the wind turbine gearbox and the reliability indicators of the gear system, which has significant advantages in terms of simulation and testing costs. Liu *et al.* proposed a fatigue reliability assessment method based on continuous-time Bayesian networks and finite element analysis, considering the failure and uncertainty of the load and material parameters on the wind turbine[25]. Horn *et al.* studied the impact of introducing a stochastic model of availability on the estimation of the lifespan of offshore wind turbines and conducted a fatigue reliability assessment of offshore wind turbines[26]. Liu *et al.* developed a new optimization model for gear transmission in wind turbine systems based on dynamic fatigue reliability sensitivity[27]. This model was used to predict the optimal structural parameters of gear transmission in wind turbine systems. In the model, the dynamic fatigue reliability of the gear transmission was evaluated based on the stress-strength interference theory.

This article focuses on the fatigue reliability of the foundation ring of wind turbines. The reliability analysis of the structure under long-term wind loads belongs to the field of structural dynamic reliability analysis, which involves two failure mechanisms: exceedance failure mechanism[28-30] and fatigue failure mechanism[31,32]. Structural fatigue failure is caused by the accumulation of damage due to the structure exceeding the safety threshold multiple times during the response process. Therefore, the probability analysis of multiple threshold crossings in stochastic processes should be considered in fatigue reliability assessment.

Based on recent advancements in the analysis of stochastic processes and multiple threshold crossings[33,34], as well as the availability of real-time monitoring data through SCADA systems to determine average wind speeds, this study employs the orthogonal expansion method[22] and the number theory method[35] to simulate the pulsating wind speed-time series. By generating the stochastic wind speed-time series, the wind load acting on the wind turbine can be calculated. The wind turbine structure is modeled using ABAQUS finite element software, and the obtained wind load-time series is applied to the model to obtain the stress-time series at the stress concentration of the wind turbine foundation ring. Considering the significant impact of the duration of the stochastic response process beyond the damage threshold (referred to as crossing-threshold duration) on the fatigue reliability of the wind turbine structure, it is important to use a structural fatigue reliability analysis method that considers the stochastic process of crossing-threshold holding time. This approach is more representative of the actual fatigue reliability analysis of the wind turbine foundation ring, and it has practical implications for engineering applications.

CALCULATIONS OF WIND SPEED-TIME SERIES AND WIND LOAD-TIME SERIES

Overview of the wind turbine engineering

ABAQUS is utilized to conduct finite element modeling and analysis of a 5 MW wind turbine generator. The main parameters of the wind turbine are as follows. The height of the generator rotor is 80 m, the diameter of the rotor is 115 m, the rated wind speed is 11.9 m/s, and the design life is 20 years. The nacelle of the turbine weighs 131.142 t. The rotor consists of three blades and a hub, with each blade' length being 55 m. The total weight of the rotor is 68.283 t, and the rated rotational speed is 14.3 rpm. The wind turbine tower is composed of three sections of variable cross-section steel tower, with geometric parameters shown in Table 1. The wind turbine foundation adopts a circular pedestal-type expanded foundation, with a ground diameter of 18.8 m and a burial depth of 3.4 m. The tower and foundation ring are made of Q345 steel, and the foundation concrete is made of C40 concrete.

Calculation of wind speed-time series

In order to obtain real-time operational condition factors of wind turbines, most wind farms are equipped with SCADA systems, which can monitor and collect data in real time, with a data collection interval of seconds. There are limitations in obtaining data through SCADA systems, such as incomplete and inaccurate data, *etc*. In order to alleviate these problems, the data used in this paper is the average wind speed v_{80} = 16.74 m/s at the rotor of the wind turbine collected by the SCADA system during normal operation within a day.

The wind speed time series at a certain height z is equal to the average wind speed plus the fluctuating wind speed time series. The average wind speed at each height is obtained using wind speed conversion formulas. The random fluctuating wind field is calculated and simulated using the orthogonal expansion method[22] and number theory point selection method[35], and the wind speed time series at a certain height z is obtained accordingly. The wind speed time series is calculated by

$$V(\theta;z,t)=\overline{V}(z)+\tilde{V}(\theta;z,t) \tag{1}$$

where $\overline{V}(z)$ is the average wind speed at height z; $\tilde{v}(\theta; z, t)$ is the pulsating wind speed-time series at height z.

In order to simplify the calculation, the tower of a 75 m high wind turbine tower is divided into 0~15, 15~45 and 45~75 m, and the wind speed at the center of the three sections is taken as the average wind speed of the tower in the section, i.e., the average wind speed at 7.5, 30 and 60 m. The conversion for the average wind speed at each height is expressed as follows.

$$\frac{\overline{V}(z)}{\overline{V}(80)}=k\left(\frac{z}{80}\right)^{\lambda} \tag{2}$$

where λ is the ground roughness coefficient; k is the conversion coefficient of different landforms. According to the "Standard for design of high-rising structure"[36], it can be seen that the wind farm is located in the landform of class B; the value of λ is 0.16, and the value of k is 1.0.

In the case where the power spectral density (PSD) function of the pulsating wind speed-time series $\tilde{v}(\theta; z, t)$ does not vary with height, the pulsating wind speed-time series $\tilde{v}(\theta; z, t)$ can generally be represented as[22]

$$\tilde{V}(\theta;z,t)=U(\theta;z)v(t) \tag{3}$$

Table 1. The geometric parameters of each tower of the wind turbine

Tower	Height (m)	Bottom outer diameter (m)	Top outer diameter (m)	wall thickness (m)
Lower section	14.86	4.5	4.5	0.05
middle section	28.315	4.5	3.9	0.05
upper section	32.102	3.9	3.07	0.02

where $U(\theta;z)$ is a random field that responds to the spatial correlation of pulsating wind speeds; $v(t)$ is a stochastic process that responds to the pulsating wind properties.

According to the Literature[22], it can be obtained that the stochastic process $v(t)$ that responds to the pulsating wind characteristics can be represented by an orthogonal expansion as

$$v(t) = \sqrt{2}\sum_{j=1}^{r}\sqrt{\lambda_j}\xi_j F_j(t) \tag{4}$$

$$F_j(t) = \sum_{n=0}^{N}\chi_{n+1}\varphi_{j,n+1}\dot{\phi}_n(t) \tag{5}$$

where N is the number of unfolding terms taking the value of 600; r is the truncation coefficient taking the value of 10 (The first 10 eigenvalues account for about 90% of the total energy, and the random variables of their corresponding eigenvalues can reflect the main probabilistic properties of the virtual pulsating wind displacement process[22]); $\chi_{n+1}(n = 1, 2\ldots, N)$ is a set of harmonic energy adjustment coefficients, which is mainly introduced to consider the error caused by truncation; λ_j is the j-th eigenvalue of the correlation matrix $\mathbf{R}$ of the stochastic process of pulsating wind speed based on the Fourier mean spectrum; $\varphi_{j,n+1}$ is the $(n+1)$-th row element of the j-th standard eigenvector $\mathbf{\Phi}_j$ of the correlation matrix $\mathbf{R}$; $\dot{\phi}_n(t)$ is the derivative of the Hartley orthogonal basis function; $\{\xi_j, j = 1, 2, 3\ldots r\}$ is a set of mutually independent standard Gaussian random vectors obtained using the number theory point selection method, in this paper $r = 10$.

For the correlation matrix $R = [\rho_{ij}]_{N\times N}$, the autocorrelation function ρ_{ij} (only related to the time interval $\tau = t_2 - t_1$) is given as follows[22]

$$\rho_{ij} = \int_0^T\int_0^T R_u(t_2 - t_1)\phi_i(t_1)\phi_j(t_2)dt_1dt_2(i, j = 1, 2, \ldots, N) \tag{6}$$

$$\phi_k(t) = \frac{1}{\sqrt{T}}cas(2k\pi t/T)(k = 0, 1, 2, \ldots N-1) \tag{7}$$

where the deterministic function $\phi_k(t)$ is the Hartley orthogonal basis function, where $cas(t) = cos(t) + sin(t)$; T is the length of time which takes the value of 600 s.

Construct the corresponding autocorrelation function of the virtual pulsating wind displacement random process $u(t)$ based on the equivalent pulsating wind characteristic random process $v(t)$, as given in[22]

$$\begin{aligned} R_u(\tau) &= \int_{-\infty}^{\infty} S_u(\omega)\exp(i\omega\tau)d\omega \\ &= \frac{A}{2\gamma}\left[\frac{\exp(-(\alpha-\gamma)|\tau|)}{\alpha-\gamma} - \frac{\exp(-(\alpha+\gamma)|\tau|)}{\alpha+\gamma}\right] \end{aligned} \tag{8}$$

where $A = 6.0k_0v_{10}^2$; $\alpha = 3.6239\frac{v_{10}}{c}$; $\beta = \gamma i$, where $\gamma = 2.6853\frac{v_{10}}{c}$; k_0 is the dimensionless surface roughness coefficient, which takes the value of 0.0033; v_{10} is the average wind speed at a height of 10 m, which can be obtained from Eq. (2); the coefficient C = 600 m; $i = \sqrt{-1}$.

Because the wind speed at the center point of each tower section and at the impeller is mainly considered, for Eq. (3), there is[22]

$$U(\theta;z) = \sum_{j=1}^{r_z} \sqrt{\lambda_{zj}}\,\xi_j(\theta) f_{zj}(z) \tag{9}$$

where $\{\xi_j(\theta), j = 1, 2, 3\ldots r_z\}$ is consistent with Eq. (4), and it is also a set of mutually independent standard Gaussian random vectors; for the building within 150 m in this paper, $r_z = 5$[22] can meet the required accuracy; $\sqrt{\lambda_{zj}}$ and $f_{zj}(z)$ are the eigenvalues and eigenfunctions of the Fredholm integral equation, satisfying[22]

$$\int_{D_z} R_{U_z}(z_1, z_2) f_{zj}(z_1) dz_1 = \lambda_{zj} f_{zj}(z_2) \tag{10}$$

$$R_{U_z}(z_1, z_2) = \exp\left(-\frac{|z_2 - z_1|}{L_z}\right) \tag{11}$$

The reaction pulsating wind characteristic stochastic process $v(t)$ and the reaction pulsating wind speed spatial correlation random field $U(\theta;z)$ where the dimensionless set of random variables $\{\xi_j, j = 1, 2, 3\ldots r\}$ and $\{\xi_j(\theta), j = 1, 2, 3\ldots r_z\}$ satisfy[22]

$$E\left[\xi_j\right] = 0 (j = 1, 2, \ldots r), E\left[\xi_i \xi_j\right] = \delta_{ij} (i, j = 1, 2, \ldots r) \tag{12}$$

$$E\left[\xi_j(\theta)\right] = 0 (j = 1, 2, \ldots r_z), E\left[\xi_i(\theta) \xi_j(\theta)\right] = \delta_{ij} (i, j = 1, 2, \ldots r_z) \tag{13}$$

where δ_{ij} is the Kronecker-delta symbol.

If the stochastic process of pulsating wind speed and its virtual wind displacement can be assumed to be the Gaussian process, then the sets of random variables $\{\xi_j, j = 1, 2, 3\ldots r\}$ and $\{\xi_j(\theta), j = 1, 2, 3\ldots r_z\}$ are both mutually independent sets of standard Gaussian random variables. Utilizing the number theory point selection method[35], a data table that provides vectors according to Literature[37] can be used to select points directly. In this paper, the MATLAB program is used to implement the number theory point selection method, and the number of selections in the hypersphere is N_{sel} = 180; i.e., 180 standard Gaussian random variable sets are obtained from the screening. Based on 180 standard Gaussian random variable groups, MATLAB software is used to write programs. Since the SCADA system collects data at one-second intervals, and wind speeds are converted to reflect the 10 m height standard in our country, we used the 10 min average annual maximum wind speed as the basic wind speed v_0; so, the pulsating wind speed simulation is performed with a time step of 1 s, over a total simulation period of 600 s. Using Eq. (3) through Eq. (13), the appropriate pulsating wind speed-time series $\tilde{V}(\theta; z, t)$ can be obtained. Four groups of excellent pulsating wind speed-time series were selected among them, and combining with Eq. (1) and Eq. (2), further calculations were performed to obtain the wind speed-time series at 7.5, 30,

60 m, and at the impeller, i.e., the wind speed-time courses acting on 0~15, 15~45, 45~75 m and the blades of the wind turbine, and the results of the calculations are shown in Figures 1-4.

Calculation of wind load-time series

The standard value of wind loads perpendicular to the surface of the wind turbine tower according to "Standard for design of high-rising structure"[36] is calculated according to

$$\begin{cases} F_{ki}=\omega_k h_i d_i \\ \omega_k=\beta_z \mu_s \mu_z \omega_0 \end{cases} \tag{14}$$

where F_{ki} is the wind load standard value of each section of the wind turbine tower; ω_k is the standard value of wind load acting on the unit projection area at the height z of the wind turbine tower; ω_0 is the basic wind pressure, which takes the value of 0.55 kN/m^2 according to the site conditions where the wind turbine is located; h_i is the height of each section of the wind turbine tower; d_i is the diameter of the center point of each section of the wind turbine tower; β_z is the wind vibration coefficient at height z; μ_z is the wind pressure height change coefficient at height z of the wind turbine tower; μ_s is the wind load body type coefficient, taking the value of 0.7. β_z and μ_z are obtained by taking values according to the specification[36].

Given the wind speed time series acting on the tower body, the corresponding wind load acting on the wind turbine tower body is calculated according to

$$\begin{cases} F_i=\omega_k h_i d_i \\ \omega_k=\mu_s \omega_p \end{cases} \tag{15}$$

where F_i is the wind load corresponding to each section of the wind turbine tower; ω_p is the wind pressure at the corresponding height z.

According to the Bernoulli's theory the relationship between wind speed and wind pressure can be obtained as

$$\omega_p = \frac{1}{2}\rho V_t \tag{16}$$

where ρ is the air density; V_t is the wind speed-time course at the impeller under normal operating conditions of the wind turbine.

For the wind load on the tower blades, it can be divided into two specific cases: normal operating conditions and extreme load conditions. Due to the obtained data in this paper being wind speeds obtained during normal operation of the wind turbine, the effects of extreme loads are not considered for now. Under normal operating conditions, the thrust force of the blade due to the wind load can be calculated according to the following equation, based on the momentum-blade element theory.

$$F_z = \frac{1}{2}\rho A C_T V^2 \tag{17}$$

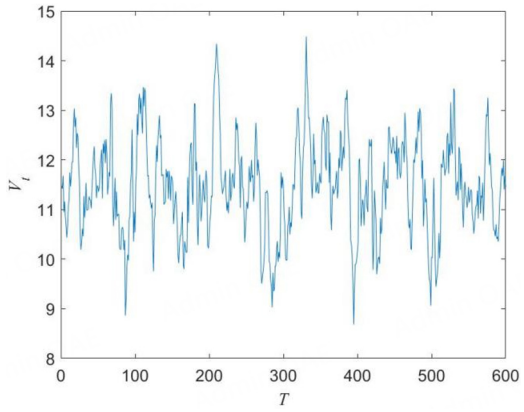

Figure 1. 0~15 m wind speed-time series.

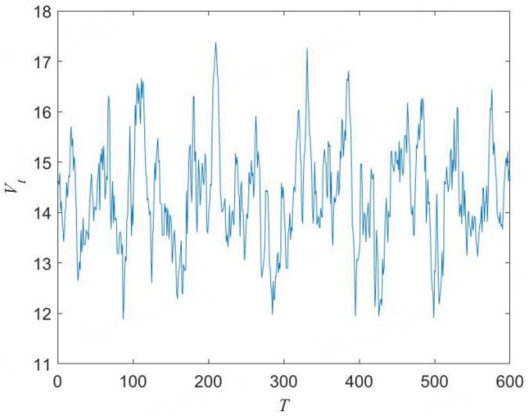

Figure 2. 15~45 m wind speed-time series.

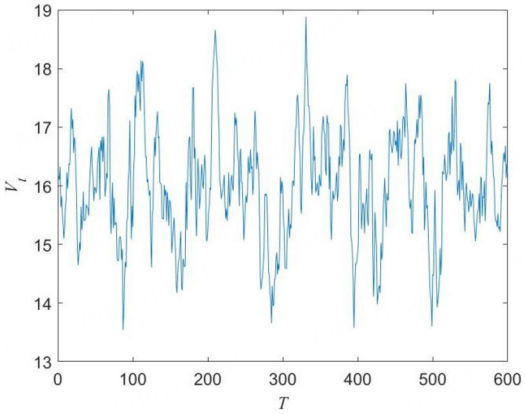

Figure 3. 45~75 m wind speed-time series.

where A is the wind turbine blade swept area; C_T is the thrust coefficient. The thrust coefficients of the wind turbine are different at different wind speeds and the thrust coefficients of this 5 MW wind turbine are given by the manufacturer as shown in Figure 5.

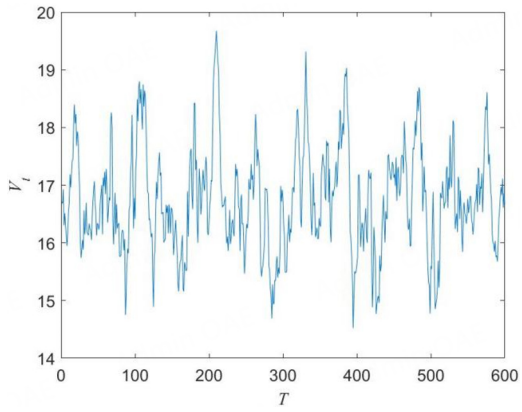

Figure 4. Wind speed-time series at the impeller under normal operating conditions of the wind turbine.

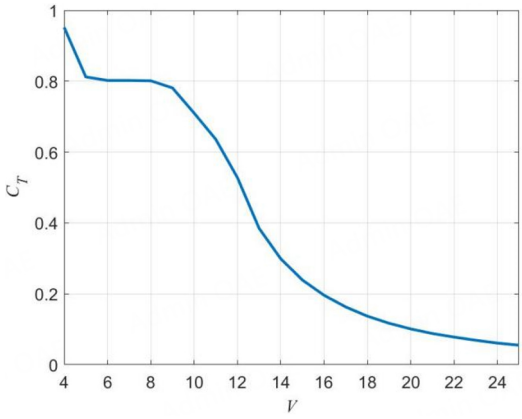

Figure 5. Thrust coefficients of the wind turbine at different wind speeds.

The wind speed-time series of the wind turbine tower at 0~15, 15~45, 45~75 m is brought into Eq. (15) respectively, and the total wind load-time series acting on each section of the tower can be calculated out, as given in Figures 6-8.

The wind speed-time series at the impeller of the wind turbine under normal operating conditions is brought into Eq. (17) to obtain its corresponding total wind load-time series, as shown in Figure 9.

NUMERICAL SIMULATION OF WIND TURBINE STRUCTURE USING ABAQUS

Establishment of wind turbine model in ABAQUS

The focus of this study is on the foundation ring, so the model has been simplified for ease of modeling, mainly divided into three major parts: (1) upper structure; (2) tower body; and (3) foundation. The upper structure consists of the hub, blades, and nacelle, while the foundation includes the concrete foundation and the foundation ring. The tower body is modeled based on the actual geometric parameters in Table 1. Considering that the vibration characteristics of the wind turbine structure mainly depend on the tower body, the modeling of the upper structure is simplified. In order to ensure that the overall stiffness and mass remain unchanged, an equivalent modeling approach is adopted. The material properties used in the equivalent modeling have a density of 258.26 kg·m^{-3}, an elastic modulus of 200 GPa, and a Poisson's ratio of 0.3. The material properties for the remaining parts are set according to their actual properties, as shown in Tables 2-3.

Table 2. Material properties

Name of material	Density ($kg \cdot m^{-3}$)	Modulus of elasticity (GPa)	The Poisson's ratio	Standard value of tensile strength (MPa)	Standard value of compressive strength (MPa)
C40 Concrete	2500	32.5	0.2	2.39	26.8
Q345 Steel	7850	200	0.3	345	345

Table 3. Steel Q345 hardening curve

Stress σ (MPa)	414	465	543	606	671	708	773
Strain ε (%)	0	0.0428	0.903	0.1384	0.1782	0.2175	0.2663

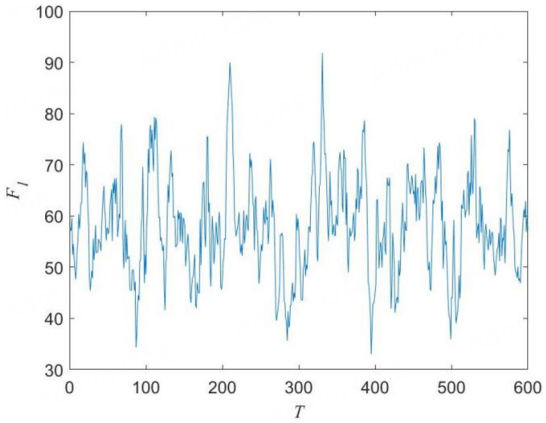

Figure 6. Total wind load acting on 0~15 m tower body-time series.

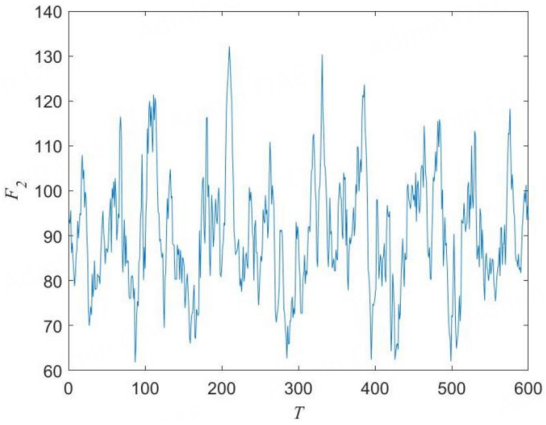

Figure 7. Total wind load acting on 15~45 m tower body-time series.

Since the focus of this study is on the fatigue reliability and fatigue life of the foundation ring, the modeling of the steel reinforcement in the concrete foundation and the modeling below the foundation are abandoned. Tie connections are used between the hub and nacelle, nacelle and tower body, and tower body and foundation ring. The concrete foundation and the foundation ring are in face-to-face contact, with Coulomb friction contact in the tangential direction and a friction coefficient of 0.35. The normal contact is treated as hard contact. Regarding the boundary conditions, the concrete foundation ground is assumed to have a fully fixed boundary condition since the modeling of the foundation is not considered. The mesh

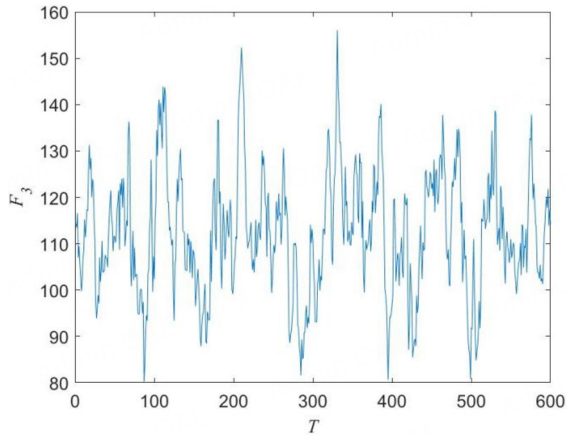

Figure 8. Total wind load acting on 45~75 m tower body-time series.

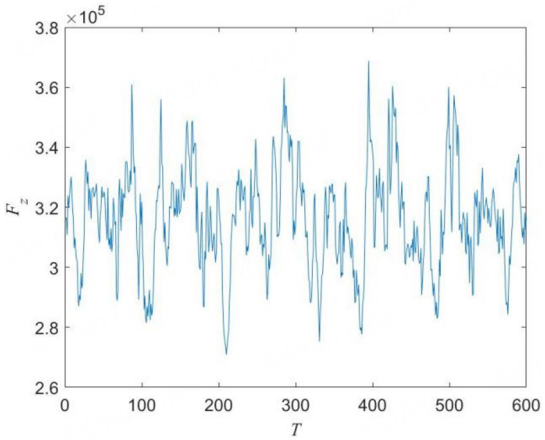

Figure 9. Total wind load acting on the impeller of the fan under normal operating conditions-time series.

division for each component is as follows: the blades and hub use solid elements C3D10, the nacelle, concrete foundation, and tower body use solid elements C3D8R, and the foundation ring uses shell elements S4R. The overall mesh division is shown in Figure 10, and the mesh division for the focus on the foundation ring is shown in Figure 11.

Since the wind speed collected in real time by the SCADA system in this study is the wind speed on the windward side, the wind load is only applied to the windward side of the turbine rotor and tower body. The total wind load received at heights of 0-15, 15-45, 45-75 m, and at the rotor is established as "amplitude" based on the corresponding relationship between time and load values. In the ABAQUS finite element software, the 75 m high tower body is divided into three sections, and reference points RP-1 to RP-3 are established at the center of each section. Each reference point is coupled with the corresponding surface of the tower body, and the loads acting on each section of the tower body are applied to the reference points. As for the total wind load-time series acting on the turbine rotor, since the main focus of the study is on the foundation ring, a concentrated load method is used to apply the load to the center of the rotor hub.

The modal analysis of the wind turbine structural model in ABAQUS

Based on the ABAQUS model established in Section "Establishment of wind turbine model in ABAQUS", in

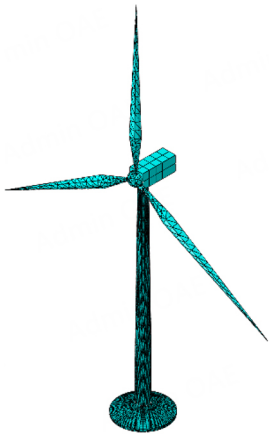

Figure 10. Overall meshing.

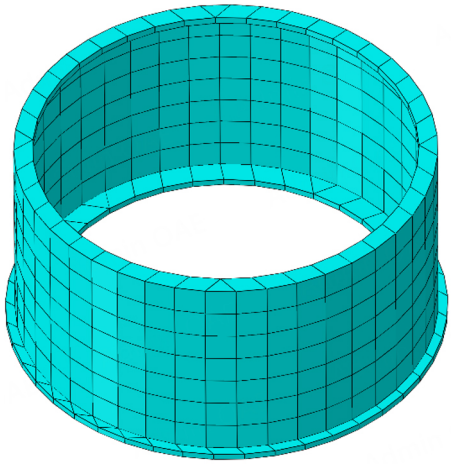

Figure 11. Foundation ring meshing.

order to ensure that the wind turbine does not collapse due to resonance between low-order natural frequencies and rotor rotation frequencies (The difference between the higher order intrinsic frequency of the wind turbine and the rotational frequency of the impeller is large, and due to the role of structural damping, the higher order part of the dynamic response attenuates very quickly), modal analysis is conducted before performing transient modal dynamic analysis in ABAQUS finite element software. Therefore, the wind turbine model is first subjected to modal analysis to obtain its low-order natural frequencies.

Modal analysis is performed in ABAQUS, without considering the influence of loads, only setting boundary conditions. This study only aims to obtain the first four natural frequencies of the wind turbine, so the subspace iteration method is used for faster calculation results. The calculated natural frequencies of the wind turbine are shown in Table 4, and the modal shapes are shown in Figure 12. From the figure, it can be observed that the low-order modal shapes of the wind turbine mainly exhibit bending and swinging forms.

The rated speed of the 5 MW wind turbine rotor is known to be 14.3 r/min. From calculations, the rotational frequency of the rotor can be determined as f = 14.3/60 Hz = 0.2383 Hz. The rotor has three

Table 4. Wind turbine first 4th order natural frequency

Ordinal number	1	2	3	4
Natural frequency (Hz)	0.37680	0.37759	0.6420	0.80267

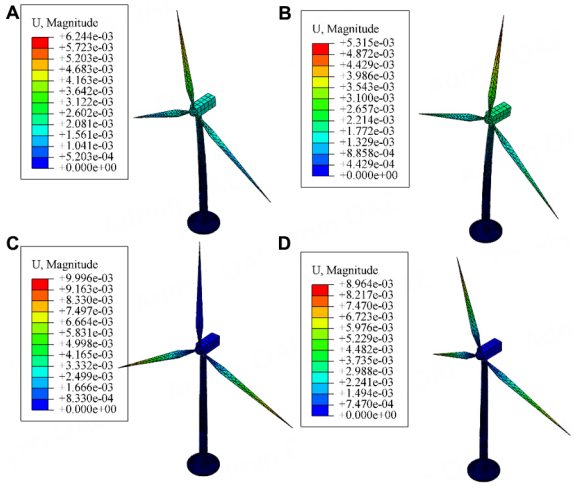

Figure 12. Wind turbine first 4th order mode shapes; (A) First-order mode shapes; (B) Second-order mode shapes; (C) Third-order mode shapes; (D) Fourth-order mode shapes.

blades, and it is known from literature[38] that the prerequisite for avoiding resonance between the wind turbine tower and the rotor is that the relative difference between the natural frequency of the tower and the rotor rotation frequency or three times the rotor rotation frequency ($3f$ = 0.7149 Hz, i.e., the passing frequency of the blades) should be greater than 10%. The relative differences between the calculated natural frequencies in Table 3 and the rotor rotation frequency are shown in Table 5, and all the relative differences are greater than 10%. Therefore, there will be no resonance between the wind turbine tower and the rotor, thus verifying the correctness of the wind turbine structure model established in this paper.

Transient modal dynamics analysis of the wind turbine model in ABAQUS

In the transient modal dynamic analysis, Rayleigh damping is considered. According to Table 3, the damping coefficients α and β corresponding to the first and second natural frequencies of the wind turbine are calculated by

$$\alpha = \frac{2\omega_1\omega_2\xi}{\omega_1 + \omega_2} \tag{18}$$

$$\beta = \frac{2\xi}{\omega_1 + \omega_2} \tag{19}$$

where ξ is the structural vibration damping ratio, which is taken as 0.05 according to the "Standard for design of high-rising structure"[36]; ω_1 and ω_2 are the circular frequencies of the 1st and 2nd vibration modes, respectively, and $\omega_i = 2\pi f_i$, f_i is the i-th order intrinsic frequencies of the wind turbine.

By substituting the first and second natural frequencies of the wind turbine from Table 3 into Eqs. (18) and (19), the calculated Rayleigh damping coefficients α = 0.11850 and β = 0.02110 can be obtained.

Table 5. Relative difference between the first 4 orders of the wind turbine

Ordinal number	1	2	3	4
Relative difference with f (%)	58.12	58.45	169.41	236.83
Relative difference with $3f$ (%)	-47.29	-47.18	-10.20	12.28

The wind load calculated in Section "Calculation of wind load-time series" is applied to the wind turbine model. Then, the Rayleigh damping coefficients α and β are input into the modal dynamics analysis step of the ABAQUS finite element software to perform transient modal dynamic response analysis, thereby obtaining the stress-time series. The stress contour map of the foundation ring, which is the main focus of the study, is shown in Figure 13. By observing the figure, it can be seen that the red region in the figure, which corresponds to the flange edge of the foundation ring, is the area with the highest stress. This is consistent with the occurrence of the highest stress area in the structure in actual engineering. The stress-time series of this maximum stress region is extracted and shown in Figure 14.

Discussion for applicability of FE model

The model used above is a 5 MW wind turbine. Because of its high power generation rate, it is more commonly used in the field of wind power generation, especially in some areas rich in wind resources (including the seaside). The dimensions and material properties of the wind turbine are obtained from the manufacturer. In performing the ABAQUS finite element modeling and analysis, the structure is modeled in a simplified manner, such as the superstructure is modeled in an equivalent manner for ease of computation and generalizability, which can be used for the study of this type of 5 MW wind turbine. This paper focuses on the fatigue reliability at the maximum stress at the edge of the flange on the base ring of a wind turbine. The fatigue reliability of the flange edge on the base ring is analyzed by the fatigue reliability calculation method considering the crossing-threshold duration, and a comparative analysis is made by the traditional method. The method is generalized and can be used for other types and sizes of wind turbine structures, and is also applicable to the calculation of stress-fatigue reliability of structures in different environments.

FATIGUE RELIABILITY ANALYSIS OF FOUNDATION RING CONSIDERING CROSSING-THRESHOLD DURATION OF RANDOM PROCESS

Stress-time histories characterized by Wiener processes

According to the "Standard for design of steel structures"[39], the stress amplitude of lower than the fatigue cut-off limit $[\Delta\sigma_L]$, that is, $\Delta\sigma = \sigma_{max} - \sigma_{min} < [\Delta\sigma_L]$, will not lead to fatigue damage. Therefore, it can be concluded that fatigue damage is mainly related to the stress amplitude, and not directly related to the maximum and minimum stress values. Therefore, the stress-time series of the maximum stress region of the foundation ring is obtained by subtracting its mean value, as shown in Figure 15. At the same time, the effect of tensile-averaged stress on fatigue damage cannot be neglected because the stress average $\sigma_m = 60.85$ MPa > 0 in the region of maximum stress in the base ring in the original Figure 14 is not zero. The stress amplitude S is to be corrected equivalently in the subsequent rainfall counting method. This stress-time series has the same stress amplitude as the original stress-time series. Therefore, this new stress-time series is used for subsequent fatigue reliability analysis.

The stress-time series of a structure under load can be considered as a stochastic process. And some stress-time histories of structures can be approximated as Wiener processes, which have the characteristics of a Wiener process. Figure 16 shows a sample curve of a Wiener process (with a duration of 1,200 and 200 s). By comparing it with the stress-time series of the new maximum stress region of the foundation ring in

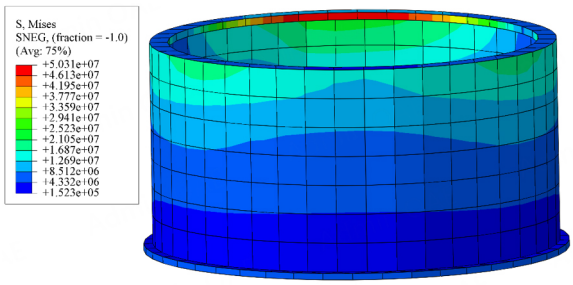

Figure 13. Stress cloud of wind turbine foundation ring.

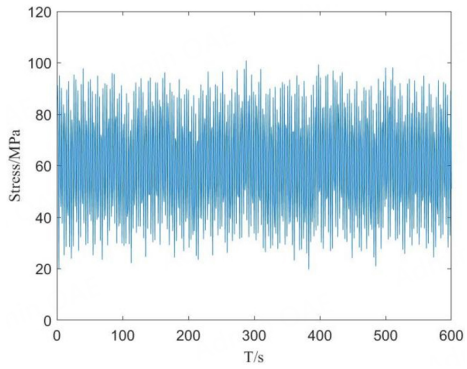

Figure 14. Stress-time series in the stress-concentrated region of the wind turbine foundation ring.

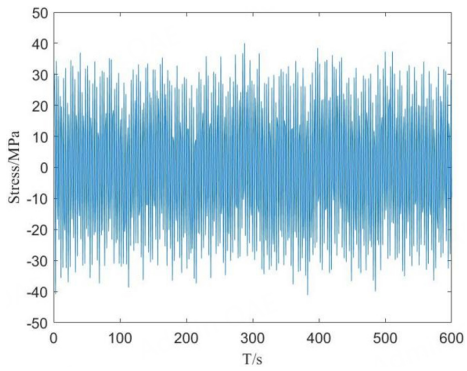

Figure 15. Stress-time series in the stress-concentration region of the modified wind turbine foundation ring.

Figure 15, it is found that the long-term Wiener process (e.g., 1,200 s) does not match the stress-time series, but the short-term Wiener process (e.g., 200 s) is more similar to the stress-time series. At the same time, the stress variation process of the maximum stress region of the foundation ring in normal operation of the wind turbine shows similarity; i.e., the entire random stress spectrum can be regarded as a repetition of typical stress-time load spectra. Therefore, it is assumed that the short-term Wiener process can be regarded as a typical stress-time spectrum block, and based on the similarity between the short-term Wiener process and the stress-time series, the stress-time series of the maximum stress region of the foundation ring can be considered as a repetition of stress-time histories based on short-term Wiener processes.

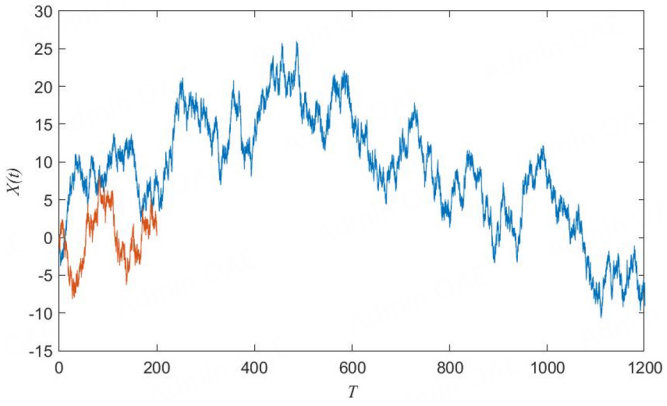

Figure 16. The sample curves for the Wiener process.

Structural fatigue reliability analysis

Based on the progress of the analysis of multiple threshold crossings of stochastic processes in recent years[33], the structural fatigue reliability analysis method considering the crossing-threshold duration of stochastic processes is used to analyze the fatigue reliability of structures. The calculation formula is as follows[40].

$$P_r = P\{x_1 < \frac{2C \cdot \int_0^q \frac{b}{\sqrt{2\pi^3 t^3}} e^{\frac{b^2}{2t}} \Gamma(0, \frac{b^2}{2t}) dt}{i \cdot N_e E(S^m) \int_0^q t \frac{b}{\sqrt{2\pi^3 t^3}} e^{\frac{b^2}{2t}} \Gamma(0, \frac{b^2}{2t}) dt}\} \tag{20}$$

where x_1 refers to the number of threshold crossings for the cyclic process of stresses within a periodic short time period t_{short}; in this paper, t_{short} =100 s; i is the number of periodic short time periods t_{short} within the normal running time length T, i.e., $i = T/t_{short}$; N_e is that the statistically obtained number of stress cycles per day is about 5.00×10^6 times; $E(S^m)$ is the m-order moment of origin of the stress amplitude S; m and C are the correlation coefficients of components and connections, according to the "Standard for design of steel structures"[39], the components and connection types are selected as Z8, take m = 3, $C = 0.72 \times 10^{12}$; q is the length of time taken for the stress to cycle once; b is the damage threshold, according to the "Standard for design of steel structures"[39], when the stress amplitude is lower than the fatigue cut-off limit will not lead to fatigue damage, so take the stress amplitude at times $N = 1 \times 10^8$ as the fatigue cut-off limit, i.e., $b = [\Delta\sigma_L]_{1\times10^8}$ = 29 MPa.

The connection between the foundation ring and the tower is made using a flange connection. The maximum stress generated at the upper flange of the foundation ring can significantly reduce the fatigue strength at the upper flange and bolt locations. The research object is selected as the location of the maximum stress at the upper flange of the foundation ring, and its stress-time series is shown in Figure 17. It is now corrected for equivalent stresses, and the material strength is taken as 345 MPa. Subsequently, the rainfall counting method is applied to this data to obtain its 16-level stress spectrum, as shown in Table 6.

According to the data in Table 6 and the member and connection correlation coefficient m = 3, it is possible to obtain:

Table 6. Statistics of stress amplitude

Amplitude/MPa	19.70	21.05	22.40	23.74	25.09	26.44	27.79	29.14
Times (×10^3)	103.45	321.84	804.60	1,011.49	965.52	413.79	114.94	183.91
Frequency	0.02069	0.06437	0.16092	0.2023	0.1931	0.08276	0.02299	0.03678
Amplitude/MPa	30.48	31.83	33.18	34.53	35.87	37.22	38.57	39.92
Times (×10^3)	149.43	333.33	160.92	195.40	149.43	34.48	22.99	34.48
Frequency	0.02989	0.06667	0.03218	0.03908	0.02989	0.0069	0.0046	0.0069

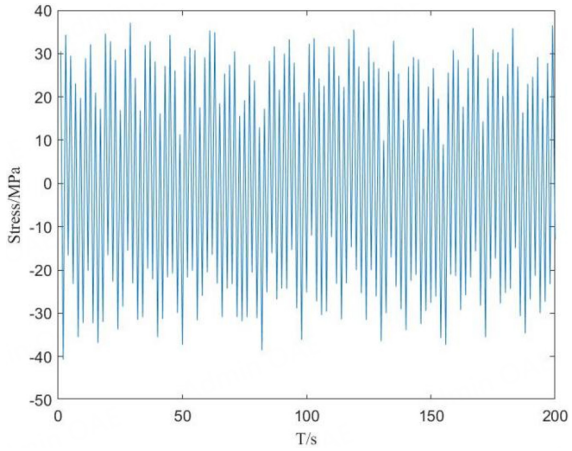

Figure 17. Stress-time series.

$$E(S^m) = 19475.048$$

x_1 is the number of times the stress cycling process crosses the damage threshold b in a periodic short time period t_{short}, which needs to be generated by simulation with the MATLAB program. Through t_{short} = 100 s, it can be obtained that in 100 s, in order to accurately require to take dt = 0.01 s, through the MATLAB program simulation to generate 10,000 standard Wiener process curves. The value of the number of crossings x_1 of this sample curve with the damage threshold b was counted, as shown in Table 7.

The next step is to calculate the value on the right side of Eq. (20), i.e., calculating $U = \frac{2C \cdot \int_0^q \frac{b}{\sqrt{2\pi^3 t^3}} e^{\frac{b^2}{2t}} \Gamma(0, \frac{b^2}{2t}) dt}{i \cdot N_e E(S^m) \int_0^q t \frac{b}{\sqrt{2\pi^3 t^3}} e^{\frac{b^2}{2t}} \Gamma(0, \frac{b^2}{2t}) dt}$ [40] to get the values as shown in Table 8.

The probability of statistically obtaining the number of crossings x_1 and the value of U in Table 8 are uniformly brought into Eq. (20). The fatigue reliability of the stress concentration area of the flange on the base ring over time can be calculated, as shown in Table 9, Figure 18. Similarly, the case of periodic short time duration of 200 s was also calculated, and its U values are shown in Table 8, and the fatigue reliability is shown in Table 10 and Figure 18.

From Figure 18, it can be observed that the fatigue reliability of the maximum stress region at the upper flange of the foundation ring decreases with time. This means that the probability of fatigue failure at the upper flange of the foundation ring grows with the service time. This also increases the probability of

Table 7. Statistics on the number of threshold crossings (t_{short} = 100 s, b = 29)

Value range of crossing times	The number of samples	Frequency
[0, 50]	6,472	64.72%
(50, 100]	2,351	23.51%
(100, 150]	890	8.9%
(150, 200]	234	2.34%
(200, 250]	45	0.45%
(250, 300]	6	0.06%
(300, 350]	2	0.02%

Table 8. Values of U (t_{short} = 100 s, t_{short} = 200 s, b = 29)

***T* (Unit: years)**	0	1	2	3	4	5	6
U (times)	-	303	151	101	76	61	50
***T* (Unit: years)**	7	8	9	10	11	12	13
U (times)	43	38	34	30	28	25	23
***T* (Unit: years)**	14	15	16	17	18	19	20
U (times)	22	20	19	18	17	16	15

Table 9. The fatigue reliability of flange stress concentration areas on the base ring (t_{short} = 100 s, b = 29)

***T* (Unit: years)**	0	1	2	3	4	5	6
Reliability (%)	100	99.98	97.24	88.45	79.24	71.37	64.72
***T* (Unit: years)**	7	8	9	10	11	12	13
Reliability (%)	59.80	56.45	53.32	50.08	48.46	46.29	44.52
***T* (Unit: years)**	14	15	16	17	18	19	20
Reliability (%)	43.79	42.05	41.22	40.27	39.39	38.46	37.59

Table 10. The fatigue reliability of flange stress concentration areas on the base ring (t_{short} = 200 s, b = 29)

***T* (Unit: years)**	0	1	2	3	4	5	6
Reliability (%)	100	99.62	87.98	72.75	61.98	54.80	48.83
***T* (Unit: years)**	7	8	9	10	11	12	13
Reliability (%)	44.82	41.76	39.49	36.86	35.71	33.77	32.50
***T* (Unit: years)**	14	15	16	17	18	19	20
Reliability (%)	31.82	30.60	29.88	29.17	28.50	27.77	26.98

detachment between the foundation ring and the upper connecting structure of the wind turbine tower. Furthermore, this leads to overall instability of the wind turbine structure, resulting in alarm shutdown or collapse. Therefore, during the service life of the wind turbine structure, it is necessary to strengthen monitoring in this area and take timely reinforcement and maintenance measures to avoid accidents and economic losses within the specified service period. In addition, comparing the cases of t_{short} = 100 s and t_{short} = 200 s in Figure 18, it can be seen that when the periodic short time duration is shorter, the calculated values are more accurate and closer to reality. This is because the Winer process of the shorter periodic short time duration is closer to the stress-time series. Meanwhile, the fatigue reliability calculated by the conventional linear cumulative damage law is shown in Figure 18. Comparison with the fatigue reliability

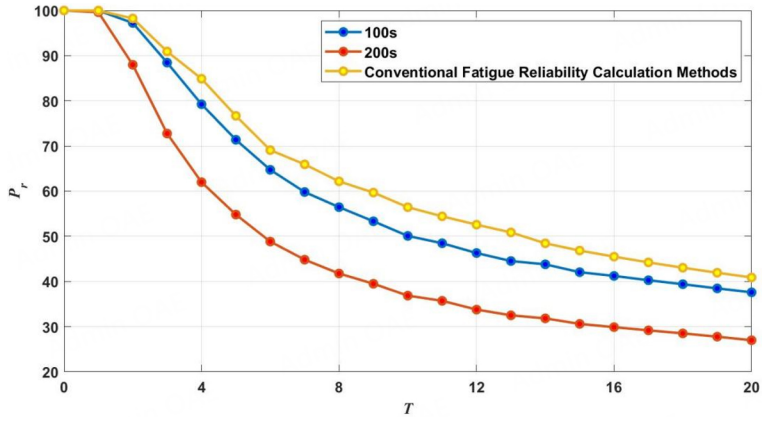

Figure 18. The fatigue reliability curves for flange stress concentration areas on the base ring (t_{short} = 100 s and 200 s, b = 29).

calculations for t_{short} = 100 s shows that they are close, but with slight differences. This is due to the fact that the method in this paper considers the effect of the duration of crossing the damage threshold and refines the effect of the stress amplitude above the damage threshold b on the fatigue damage. In contrast, the traditional method simply considers that the stress causes a fixed amount of damage to the structure every cycle, which undoubtedly leads to a large error in the calculation results[40].

CONCLUSIONS

Based on real-time monitoring data from the SCADA system, this paper combines the ABAQUS finite element software for modeling and a new structural fatigue reliability analysis method that considers the stochastic process of exceeding the threshold duration. The fatigue reliability of the maximum stress at the upper flange of the foundation ring of the wind turbine structure under normal operating conditions was calculated. The main research work and conclusions are as follows.

(1) Under normal operating conditions, the wind speed time series of each tower section is calculated by wind speed exponential model, orthogonal expansion method of random pulsating wind field and number theory point selection method in number theory, and then the wind load time series of each tower section and blade is calculated using the wind load calculation formula of standard for design of high-rising structures and the momentum-leaf vein theory. The wind loads are determined based on the real-time wind speed data collected by the SCADA system, so it should be a more reliable result.

(2) Establish a simplified model in ABAQUS finite element software in line with the engineering profile. The reasonableness of the structural model of the wind turbine was first verified by modal analysis. Subsequently, the wind load is applied to the model for instantaneous modal dynamics analysis to obtain the structural stress time course. The results show that the maximum stress region of the foundation ring is located at the edge of the upper flange, which is consistent with the engineering reality.

(3) Fatigue reliability in the region of maximum stress in the base ring is calculated using a structural fatigue reliability analysis method that considers random processes' crossing-threshold duration. The results are compared with those of the traditional method to demonstrate the superiority and reasonableness of the method that takes into account the calculation of crossing-threshold durations.

DECLARATIONS

Authors' contributions

Conceptualization, methodology, supervision: Zhang Z
Formal analysis, writing-original draft preparation: Liu Y
Investigation, writing-review and editing: Li W

Availability of data and materials

The data are available from the corresponding author upon reasonable request.

Financial support and sponsorship

This work was jointly supported by the Talent Recruitment Project of Hunan Province, China (grant no. 2023TJ-Z17), National Natural Science Foundation of China (grant no. 52478130), Regional Scientific and Technological Cooperation and Exchange Project of Hunan Association for Science and Technology (2024SKX-KJ-09).

Conflicts of interest

All authors declared that there are no conflicts of interest.

Ethical approval and consent to participate

Not applicable.

Consent for publication

Not applicable.

REFERENCES

1. de Azevedo HDM, Araújo AM, Bouchonneau N. A review of wind turbine bearing condition monitoring: state of the art and challenges. *Renew Sustain Energy Rev* 2016;56:368-79. DOI
2. Kusiak A, Li W. The prediction and diagnosis of wind turbine faults. *Renew Energy* 2011;36:16-23. DOI
3. Yang W, Tavner PJ, Crabtree CJ, Wilkinson M. Cost-effective condition monitoring for wind turbines. *IEEE Trans Ind Electron* 2010;57:263-71. DOI
4. Mcmillan D, Ault GW. Condition monitoring benefit for onshore wind turbines: sensitivity to operational parameters. *IET Renew Power Gen* 2008;2:60-72. DOI
5. Meng D, Yang H, Yang S, et al. Kriging-assisted hybrid reliability design and optimization of offshore wind turbine support structure based on a portfolio allocation strategy. *Ocean Eng* 2024;295:116842. DOI
6. Meng D, Yang S, Yang H, De Jesus AMP, Correia J, Zhu SP. Intelligent-inspired framework for fatigue reliability evaluation of offshore wind turbine support structures under hybrid uncertainty. *Ocean Eng* 2024;307:118213. DOI
7. Meng D, Yang S, de Jesus AMP, Zhu SP. A novel kriging-model-assisted reliability-based multidisciplinary design optimization strategy and its application in the offshore wind turbine tower. *Renew Energy* 2023;203:407-20. DOI
8. Meng DB, Zhu SP. Multidisciplinary design optimization of complex structures under uncertainty. Boca Raton: CRC Press; 2024. DOI
9. Nilsson J, Bertling L. Maintenance management of wind power systems using condition monitoring systems - life cycle cost analysis for two case studies. *IEEE Trans On Energy Conver* 2007;22:223-9. DOI
10. Kusiak A, Verma A. A data-driven approach for monitoring blade pitch faults in wind turbines. *IEEE Trans Sustain Energy* 2010;2:87-96. DOI
11. Gill S, Stephen B, Galloway S. Wind turbine condition assessment through power curve copula modeling. *IEEE Trans Sustain Energy* 2012;3:94-101. DOI
12. Kusiak A, Verma A. Monitoring wind farms with performance curves. *IEEE Trans Sustain Energy* 2013;4:192-9. DOI
13. Zaher A, Mcarthur SDJ, Infield DG, Patel Y. Online wind turbine fault detection through automated SCADA data analysis. *Wind Energy* 2009;12:574-93. DOI
14. Garcia MC, Sanz-Bobi MA, del Pico J. SIMAP: intelligent system for predictive maintenance: application to the health condition

monitoring of a windturbine gearbox. *Comput Ind* 2006;57:552-68. DOI
15. Yang W, Court R, Jiang J. Wind turbine condition monitoring by the approach of SCADA data analysis. *Renew Energy* 2013;53:365-76. DOI
16. Zhang S, Lang ZQ. SCADA-data-based wind turbine fault detection: a dynamic model sensor method. *Control Eng Pract* 2020;102:104546. DOI
17. Zhang F, Wen Z, Liu D, Jiao J, Wan H, Zeng B. Calculation and analysis of wind turbine health monitoring indicators based on the relationships with SCADA data. *Appl Sci* 2020;10:410. DOI
18. Tang M, Chen W, Zhao Q, et al. Development of an SVR model for the fault diagnosis of large-scale doubly-fed wind turbines using SCADA data. *Energies* 2019;12:3396. DOI
19. Liu X, Du J, Ye ZS. A Condition monitoring and fault isolation system for wind turbine based on SCADA data. *IEEE Trans Ind Inf* 2022;18:986-95. DOI
20. Velarde J, Mankar A, Kramhøft C, Sørensen JD. Probabilistic calibration of fatigue safety factors for offshore wind turbine concrete structures. *Eng Struct* 2020;222:111090. DOI
21. Wang K, Ji C, Xue H, Tang W. Fatigue damage characteristics of a semisubmersible-type floating offshore wind turbine at tower base. *J Renew Sustain Energy* 2016;8:053307. DOI
22. Fu B, Zhao J, Li B, et al. Fatigue reliability analysis of wind turbine tower under random wind load. *Struct Saf* 2020;87:101982. DOI
23. Zhu D, Ding Z, Huang X, Li X. Probabilistic modeling for long-term fatigue reliability of wind turbines based on Markov model and subset simulation. *Int J Fatigue* 2023;173:107685. DOI
24. Li M, Luo Y, Xie L, Tong C, Chen C. Fatigue reliability assessment method for wind power gear system based on multidimensional finite element method. *J Risk Reliab* 2024;238:540-58. DOI
25. Liu Z, He Z, Tu L, Liu X, Liu H, Liang J. A fatigue reliability assessment approach for wind turbine blades based on continuous time Bayesian network and FEA. *Qual Reliab Eng* 2023;39:1603-21. DOI
26. Horn JT, Leira BJ. Fatigue reliability assessment of offshore wind turbines with stochastic availability. *Reliab Eng Syst Saf* 2019;191:106550. DOI
27. Liu G, Liu H, Zhu C, Mao T, Hu G. Design optimization of a wind turbine gear transmission based on fatigue reliability sensitivity. *Front Mech Eng* 2021;16:61-79. DOI
28. Zhang Z, Zhou M, Fang M. First-passage probability analysis of Wiener process using different methods and its applications in the evaluation of structural durability degradation. *Eur J Environ Civ Eng* 2021;25:1763-81. DOI
29. Roberts JB. First-passage probabilities for randomly excited systems: diffusion methods. *Probabilist Eng Mech* 1986;1:66-81. DOI
30. Zhang Z, Liu M, Zhou M, Chen J. Dynamic reliability analysis of nonlinear structures using a Duffing-system-based equivalent nonlinear system method. *Int J Approx Reason* 2020;126:84-97. DOI
31. Pastorcic D, Vukelic G, Bozic Z. Coil spring failure and fatigue analysis. *Eng Fail Anal* 2019;99:310-8. DOI
32. Weibring M, Gondecki L, Tenberge P. Simulation of fatigue failure on tooth flanks in consideration of pitting initiation and growth. *Tribol Int* 2019;131:299-307. DOI
33. Zhang Z, Liu X, Zhang Y, Zhou M, Chen J. Time interval of multiple crossings of the Wiener process and a fixed threshold in engineering. *Mech Syst Signal Proc* 2020;135:106389. DOI
34. Zhang Z, Zhao C, Zhao Z, Wang F, Zhao B. Structural fatigue reliability evaluation based on probability analysis of the number of zero-crossings of stochastic response process. *Eng Fail Anal* 2023;143:106923. DOI
35. Liu G, Gao K, Law SS. An improved sieve point method for the reliability analysis of structures. *Probabilist Eng Mech* 2020;62:103087. DOI
36. National Standard of the People's Republic of China. Standard for design of high-rising structures (GB50135-2019). Beijing: China Architecture Industry Press; 2019. Available from: https://www.gbstandards.org/GB_standard_english_3.asp?code=GB%2050135-2019&id=45634 [Last accessed on 26 Sep 2024].
37. Gao K, Liu G, Tang W. High-dimensional reliability analysis based on the improved number-theoretical method. *Appl Math Model* 2022;107:151-64. DOI
38. Niu Q. New energy technologies-wind energy technology. Beijing: Science Press; 2009. Available from: https://ss.zhizhen.com/detail_38502727e7500f268a9ccc00f75bb01ccfc384332d18b1e11921b0a3ea25510134114c969f2eae5c8619c3781aeff6c1ed60753c1335db4b2ac4765c2ca0e502d2822a9bb48c12c32752f14c8ebc102a [Last accessed on 26 Sep 2024].
39. National Standard of the People's Republic of China. Standard for design of steel structures (GB 50017-2017). Beijing: China Architecture & Building Press; 2017. Available from: https://www.chinesestandard.net/PDFOpenLib/GB50017-2017EN-P27P-H22684H-191296.pdf [Last accessed on 26 Sep 2024].
40. Zhang Z, Liu Y, Wang L, Li W, Ma G. Probability analysis of duration of stochastic process exceeding fixed threshold and its application on structural cumulative damage and fatigue reliability evaluation. *Civ Eng* 2024;10:04024007. DOI